arXiv:1610.03185v1 [cond-mat.mtrl-sci] 11 Oct 2016

A large enhancement of carrier mobility in phosphorene by introducing hexagonal boron nitride substrate

Jiafeng Xie, Z. Y. Zhang, D. Z. Yang, M. S. Si*, and D. S. Xue

Key Laboratory for Magnetism and Magnetic Materials of the Ministry of Education, Lanzhou University, Lanzhou 730000, China

Xiaohui Deng

Department of Physics and Electronic Information Science, Hengyang Normal University

(Dated: October 12, 2016)

Abstract

Just recently, it is reported experimentally that the carrier mobility in phosphorene can be significantly enhanced on hexagonal boron nitride (h-BN) substrate. This is a big step towards the practical device applications because carrier mobility determines the power dissipation and switching speed of electronic devices. Also importantly, rich unusual physical phenomena can only be probed under a certain high carrier mobility. Unfortunately, the underlying mechanism about the enhanced carrier mobility is not well understood. In this study, we estimate the carrier mobility of phosphorene on h-BN substrate (P/h-BN) within the framework of the phonon-limited scattering model at first-principles level. Our results are generic. As a high-κ dielectric material, h-BN also possesses excellent mechanical property of a high two-dimensional elastic modulus. P/h-BN did inherit the high elastic modulus of h-BN, leading to the enhanced carrier mobility in phosphorene. Thanks to the weak van der Waals interactions between the layers, the unique electronic properties of phosphorene are almost perfectly preserved near the Fermi level, guaranteeing the superior transport in P/h-BN. Our findings offers a new perspective to improve the carrier mobility in phosphorene or other 2D materials based field effect transistors.

I. INTRODUCTION

Phosphorene, isolated from black phosphorus, is presently attracting immense research interest due to its tantalizing properties, which are not present in the bulk counterpart [1]. As a promising semiconductor, phosphorene exhibits a considerable direct band gap, which is in contrast to gapless graphene [2]. Compared to monolayer of transition metal dichalcogenides with direct band gaps, carrier mobility of phosphorene behaves in a more superior manner [3, 4]. Carrier mobility is an important parameter for semiconducting materials as it dominates the power dissipation and switching speed [5]. Thus, the phosphorene based device may offer a new opportunities to promote the desire of electronics and optoelectronics in the post-silicon era [6]. And many people in the community are looking different aspect on phosphorene to the enhancement of carrier mobility in phosphorene.

In experiment, phosphorene field effect transistors (FETs) were first synthesized on a SiO_2/Si substrate. The hole carrier mobility reaches as high as 286 $cm^2V^{-1}s^{-1}$ at room temperature with $\sim$4 nm phosphorene film [2]. In order to further enhance the carrier mobility, Li and coauthors used the flat hexagonal boron nitride (h-BN) to confine the two-dimensional (2D) electron gas within phosphorene, increasing the carrier mobility up to 400 $cm^2V^{-1}s^{-1}$ with $\sim$1 nm phosphorene film [7]. It should be noticed that the hole carrier mobility in Ref. [2] with $\sim$1 nm film is less than 24 $cm^2V^{-1}s^{-1}$. Thus, the work in Ref. [7] is a big step for the actual device applications since the h-BN induce near 20 times enhancement of hole mobility. Moreover, rich unusual physical phenomena, such as quantum oscillations and quantum Hall effect [8], can only be probed in phosphorene FETs under a certain high carrier mobility. But, the mechanism of the enhanced carrier mobility is not well understood. We notice in passing that other groups reported higher carrier mobilities in phosphorene FETs, but the reasons are attributed to fewer layers and lower temperatures taken in their experiments [9, 10]. This is not the focus of this work.

Theoretically, Ref. [11] demonstrated that the carrier mobility can be enhanced by modifying the dielectric environment. The high-κ dielectric materials would increase the damping of Coulombic scattering, resulting in a higher carrier mobility. But, this is not the case of graphene. Ponomarnenko and colleagues experimentally observed no obvious enhancement in carrier mobility of graphene on different dielectric substrates [12]. Owing to the confined 2D electron gas, Ref. [13] considered that graphene holds a strong surface phonon scatter-

ing, washing out the partial screening of Coulombic scattering [13]. In this perspective, the enhanced carrier mobility cannot be simply ascribed into a single model for all 2D layered materials. It naturally raises the crucial question that why the h-BN substrate can enhance the carrier mobility in phosphorene.

To resolve the puzzle, we construct the heterostructure of phosphorene/h-BN (P/h-BN) to mimic the experimental model at first-principles level. The obtained results are directly compared with those of phosphorene. It is found that the enhanced carrier mobility arises from the increased 2D elastic modulus, which are inherited from the h-BN substrate. At the same time, the unique electronic properties of phosphorene are well preserved in P/h-BN due to the weak van der Waals (vdW) interactions between phosphorene and h-BN. Our finding allows the control of enhancing carrier mobility in phosphorene field effect transistors, which is essential in the design of new devices based on different dielectric substrates.

II. METHODS

Our first-principles calculations are performed through using the siesta package within the framework of density functional theory (DFT) [14]. To study phosphorene on h-BN substrate, we use the generalized gradient approximation for the exchange and correlation potential as proposed by Perdew-Burk-Ernzerhof (PBE) [15]. As the vdW interactions are important in predicting the stable stacking of 2D layered materials, the optB88-vdW functional is employed in the realistic calculations [16]. For comparison, three other functionals of LDA [17], vdW-DF2 [18], and C09 [19] are taken to estimate the interlayer binding energy of P/h-BN heterostructure. The plane wave energy cutoff is set to be 210 Ry to ensure the convergence of total energy. The reciprocal space is sampled by a fine grid of $11\times5\times1$ k-point in the Brillouin zone. Structural relaxations were performed until the force on each individual atom is less than 0.01 eV/Å. The optimized double-ζ orbitals including polarization orbitals are employed to describe the valence electrons.

III. FORMALISM

To theoretically estimate the carrier mobility of 2D layered materials is not an easy task as it always involves many scattering processes, such as the charged-impurity scattering, the

phonon scattering as well as the Coulombic scattering [11, 20, 21]. For simplicity, we take the so-called phonon-limited scattering model to calculate the carrier mobility of the 2D heterostructure of P/h-BN, which reads [22–25]

$$\mu_{2D} = \frac{e\hbar^3 C_{2D}}{k_B T m^* m_a^* E_i^2}, \tag{1}$$

where e is the electron charge, $\hbar$ the reduced Plank's constant, k_B the Boltzmann constant and T the temperature, m^* (m_a^*) the (averaged) effective mass with respect to the transport direction. E_i the deformation potential constant of valence band maximum (VBM) for hole or conduction band minimum (CBM) for electron along the transport direction. The latter two quantities are closely related to band structures. m^* is referred as the second derivative of VBM or CBM band relative to crystal momentum and the averaged effective mass is determined by $m_a^* = \sqrt{m_x^* m_y^*}$. Whereas, E_i is decided by the shift of VBM or CBM band in response to the strain applied along the transport direction. In this regard, we expect phosphorene dominates these two quantities as phosphorene holds a sizable direct band gap and other excellent intrinsic electronic properties including effective mass and deformation potential. C_{2D} is the 2D elastic modulus of the longitudinal strain in the propagation directions of the longitudinal acoustic (LA) wave. It is a purely mechanical property. As a high-κ dielectric material, h-BN can modify the dielectric environment. Moreover, the flat h-BN possesses a higher C_{2D} and may increase the carrier mobility, as expected in Eq. (1), if the P/h-BN heterostructure inherits the C_{2D} of h-BN.

IV. ELECTRONIC PROPERTIES OF P/h-BN

To mimic the experimental model, we construct the heterostructure of P/h-BN by extending h-BN with 1×4 unit cells to match the fixed phosphorene with 1×3 unit cells during the geometric optimization, as displayed in Fig. 1(a). In this way, the obtained unit cell of P/h-BN heterostructure has a minimum initial mismatch of ∼3% [26, 27]. It is well known that the stacking manner plays a crucial role in electronic properties of heterostructure. For diminishing this uncertainty in our calculations, we firstly search various stackings of P/h-BN for the most stable one as our starting point. Based on the most stable stacking, we respectively shift phosphorene relative to h-BN along the armchair (x) and zigzag (y) directions. The corresponding energy curves are plotted in Fig. 1(b). As can be seen, when

the shift is along the x direction, it needs to overcome a large energy barrier as the puckered structure of phosphorene is involved (see the bottom panel of Fig. 1(a)). By contrast, the energy barrier related to the y-direction shift is quite small. This is because the flat h-BN dominates the energy curve and no obvious change in configuration occurs during this shift process. We also notice that the maximum energy barrier appears at the shift of around 5%, which was not observed in P/graphene heterostructure [28]. At this position, we find that the P atoms of phosphorene are very close to the N atoms of h-BN. Since the residual charges of h-BN largely reside in the N atoms, the Coulomb interactions between the layers are increased, giving rise to a maximum energy barrier.

In order to accurately estimate the interlayer binding of P/h-BN heterostructure, we take five exchange-correlation functionals in our simulations, as shown in Fig. 1(c). Without the vdW correlations, the functionals of PBE and LDA cannot assess rightly the interlayer coupling. The PBE underbinds and increases the interlayer spacing, while the LDA overbinds and reduces the interlayer spacing. Even if the vdW correlation is taken into account, the results are still not converged. The vdW-DF2 method gives an interlayer spacing larger than 3.7 Å, leading to a reduced binding energy of around 35 meV. The advanced version of vdW correlation, that is optB88-vdW, seems to be suited for the case of P/h-BN heterostructure. The obtained interlayer spacing is around 3.5 Å and the binding energy is around 44 meV, which are in good agreement with previous calculations [29, 30]. Based on the same functional of optB88-vdW, the binding energies of bilayer phosphorene and bilayer h-BN are ∼55 meV [31, 32] and ∼63 meV [33], respectively. This means the interlayer vdW interaction between phosphorene and h-BN is weaker than those in both bilayer phosphorene and bilayer h-BN. Such a weak coupling would preserve the electronic properties of phosphorene near the Fermi level in P/h-BN heterostructure. It is also found that this interlayer coupling is comparable to that of P/graphene [28, 30]. In addition, the vdW functional of C09 produces very similar results to those of optB88-vdW. It is reasonably believed that the optB88-vdW functional can evaluate the interlayer coupling of the heterostructure of P/h-BN at first principle calculation level. And it is thus used for the next calculations. Certainly, more accurate results can be obtained by quantum Monte Carlo method [34], but the computational cost is beyond our tolerance.

Next, we check whether the P/h-BN heterostructure indeed inherited the electronic properties of phosphorene. For comparison, the band structure of phosphorene is calculated, as

shown in Fig. 2(a). It has a direct band gap of around 0.9 eV at the Γ point. The bands of CBM and VBM have a stronger dependence on the crystal momentum along the Γ-X (armchair) direction than that along the Γ-Y (zigzag) direction. All the electronic properties mentioned above are well in line with those reported by Liu and coauthors [2]. When phosphorene is placed on h-BN substrate, the calculated band structure is displayed in Fig. 2(b). It can be seen that the bands near the Fermi level are almost the same as those of phosphorene, which is also verified by the PDOS, as shown in Fig. 2(c). In the energy range from -1.5 eV to 2.0 eV, the P-PDOS does not overlap with the B- and N-PDOS, indicating a very weak coupling between phosphorene and h-BN. Certainly, these two band structures also reveals some slight differences. For example, more bands of CBM are degenerate at the Γ point in comparison with phosphorene, resulting from the stacking effect of phosphorene on h-BN substrate. This means that the CBM bands are very sensitive to the external perturbation, in line with previous theory [35]. In P/h-BN heterostructure, since more bands are introduced by the h-BN substrate, the interactions between the bands are enhanced. Such band interactions push the VBM bands of phosphorene closer to each other and make them highly degenerate at the Γ point. As stated by Herring [36], this degeneracy is accidental because bands could degenerate at some specially crystal points perturbed by external stimulation. We also noted that the degeneracy reported by Hu and coauthors [37] is smaller than that of our model. This is because the structure of phosphorene is relaxed during the geometry optimization in Hu's work, which is in contrast to the fixed one in our case. Another effect from the h-BN substrate is the increased band gap of P/h-BN. Wider band-gap h-BN introduces an extra energy of around 0.1 eV into the band gap of P/h-BN heterostructure. Except for the above mentioned two slight differences, the P/h-BN heterostructure almost perfectly inherits the electronic properties of phosphorene near the Fermi level as we expected.

According to the effective-mass theorem [38], the effective mass is associated with the band structure via $1/m_n^* = (\partial^2/\hbar^2\partial k^2)V_n(k)$ with $V_n(k)$ being the band energy of the nth band at crystal momentum k. This means that the effective mass of carriers largely depends on the band curvatures of VBM or CBM. Since the bands near the Fermi level of P/h-BN heterostructure are almost the same as those of phosphorene, their effective masses should be similar. As illustrated in Table I, the introduced h-BN substrate only has an effect on the effective masses along the Γ-Y direction, arising from the enhanced band interactions

along this direction. The effective mass for electron decreases from 1.12 m_0 in phosphorene to 0.43 m_0 in P/h-BN along the Γ-Y direction. The similar trend is also observed in the hole carrier along this direction. By contrast, the effective masses along the Γ-X direction are nearly unchanged, yielding a reduced transport anisotropy compared to phosphorene.

Since the mobility μ is inversely proportional to the square of deformation potential E_i^2, the deformation potential is another key factor to act on the carrier mobility, which is in connection with the band structure through $E_i = \Delta V_i/(\Delta l/l_0)$ with V_i being the energy change of the ith band under cell compression or dilatation of Δl and l_0 the lattice constant. According to our calculations, though some deformation potentials are influenced by the stacking of h-BN layer, most of the deformation potentials for both electron and hole in P/h-BN are unchanged compared to those of phosphorene (see Table I for more details). Within the framwork of longitudinal acoustic phonon perturbation, the dielectric function $\epsilon(\omega, q)$ is connected to the deformation potential E_i via $\Delta E_i = E_i[\epsilon^{-1}(\omega, q) - 1]$. According to the analysis suggested by Pollak and coauthors [39], the main contribution to the $\epsilon(\omega, q)$ is the transitions from the VBM bands to the CBM bands. Thus, the introduced h-BN substrate cannot change the dielectric environment of phosphorene. This is because phosphorene dominates the VBM and CBM bands of P/h-BN, leaving the deformation potentials nearly unchanged. In this perspective, we can easily exclude the enhanced carrier mobility in the P/h-BN heterostructure from the increased damping of Coulombic scattering [11]. Unavoidable, two deformation potentials are not unchanged, the deformation potential for electron along x direction is increased ∼0.8 eV, while that for hole along y direction is decreased ∼0.3 eV. According to the Eq. (1), the small deformation potential make a different in high carrier mobility. From this point, the electron velocity is suppressed by the h-BN layer, while the hole velocity is accelerate. However, the realization is not that straightforward. As shown in Tab. I, the electron mobility is higher than that of hole along x direction. Whereas, along y direction, electron mobility loses this advantage. This is because the carrier mobility is not only sensitive to the electronic properties, but also related to the mechanics. In the following, we will demonstrate the power of h-BN substrate on the enhancement of carrier mobility from another viewpoint.

V. 2D ELASTIC MODULI OF P/h-BN

As a high-κ dielectric material, h-BN enters current researches with a main focus on its quantum confinement. For example, other not-flat layered materials can be confined on flat h-BN substrate through vdW stacking, usually appear promising properties such as high carrier mobility [40, 41] . By contrast, it is always neglected that its mechanical property also contribute to the 'high mobility'. In fact, the elastic property of h-BN has a big effect on the charge transport of vdW heterostructures. This is really the case of P/h-BN heterostructure. As shown in Table I, once the substrate of h-BN is introduced, the 2D elastic moduli of P/h-BN are significantly improved: C_{x-2D} increases from ∼30 Jm^{-2} to ∼320 Jm^{-2} and C_{y-2D} from ∼96 Jm^{-2} to ∼370 Jm^{-2}. This directly induces the enhancement of carrier mobility according to Eq. (1). For example, the electron moblity along the x direction is about five times of that of phosphorene. It is also noticed that the carrier mobilities of electron are smaller than those of hole along the y direction, which are in agreement with the experimental results [7]. Thus, the enhanced carrier mobility in the P/h-BN heterostructure is realized via the increased C_{2D}. To understand the underlying mechanism of how the carrier mobility can be enhanced, we will compare the 2D elastic moduli of the three materials, i.e., P/h-BN, phosphorene and h-BN, as follow.

The 2D elastic modulus, C_{2D}, can be obtained through fitting the expression $(E - E_0)/S_0 = C_{2D}(\Delta l/l_0)^2/2$, where E is the total energy and S_0 is the equilibrium lattice volume (the xy surface area) for a 2D material. First, we estimate the C_{2D} of phosphorene, as shown in Fig. 3. The strain energy density curve for the x-direction strain is obviously lower than that for the y-direction strain, resulting from the structural anisotropy of phosphorene. The 2D elastic moduli are $C_{x-2D} = 30.24$ Jm^{-2} and $C_{y-2D} = 96.16$ Jm^{-2}, in good agreement with previously reported values [4]. Then, we study the 2D elastic moduli of P/h-BN heterostructure. As can be seen in Fig. 3, the strain energy density curves for P/h-BN heterostructure are largely promoted in comparison with phosphorene. Under tension in the range of 0% to 2%, the curve of x-direction is slightly different from that of y-direction. By contrast, this difference disappears under compression. This means that the P/h-BN heterostructre partially preserve the structural anisotropy of phosphorene. Such transport anisotropy only under tension has not been reported in previous literatures. By fitting these curves, two slightly different 2D elastic moduli of $C_{x-2D} = 321.41$ Jm^{-2} and

$C_{y-2D} = 369.86$ Jm^{-2} are easily obtained, which are larger than those of phosphorene, but are comparable to those of h-BN. For h-BN, two identical 2D elastic moduli of $C_{2D} = 292.34$ Jm^{-2} are obtained, in accordance with experimental and other theoretical reports [42–44]. Actually, as shown in Fig. 3, the curves of P/h-BN are roughly the superposition of h-BN and phosphorene, in which h-BN dominates. This means that the P/h-BN heterostructure inherits well the elastic property, that is the 2D elastic modulus, of h-BN, inducing the enhanced carrier mobility in phosphorene. According to our results, further improving the carrier mobility requires a flat substrate which is a 2D layered material itself with higher 2D modulus. Future research can test this prediction.

VI. MODEL CHEACK

As it is known that the phonon-limited scattering model has its validity limits [45]. To intuitively validate the accuracy of our methods, the calculated phonon spectra of monolayer phosphorene, h-BN, and P/h-BN heterostructure are shown in Fig. 4. In order to be more comparable, the supercell are used in phonon calculations of phosphorene. With 12 atoms, phosphorene has 36 vibration branches in its phonon spectra (Fig. 4(a)), which are in good agreement with previous studies [46, 47]. As it can be seen, there are 3 acoustic branches: inplane transverse acoustic (TA) and the LA mode and the out-of-plane acoustic (ZA) mode, and 33 optical phonon branches. Fig. 4(b) shows the vibration spectra of h-BN with 16 atoms in the same supercell of phosphorene [48, 49]. Comparing with phosphorene, h-BN exhibit higher vibration frequencies, both acoustic modes and optical modes. This is because the B-N bonds are shorter in length and stronger in polarity than P-P bonds. The larger slopes of the LA branches near Γ of h-BN indicate the quicker sound speed and larger in-plane stiffness. Also, the gap of h-BN vibration (stop band) is smaller than that of phosphorene, indicating that h-BN have larger thermal conductivity [50]. Next, we focus on the frequencies of lattice vibrational modes of P/h-BN heterostructure shown in Fig. 4(c). It can be seen that the P/h-BN heterostructure inherit the phonon properties of h-BN. Due to the phonon vibration of h-BN, more vibration modes are induced to in P/h-BN heterostrucuture, and a small stop band. And the h-BN substrate also induces larger elastic modulus to P/h-BN heterostructure. Thus the carrier mobility in P/h-BN heterostructure the carrier mobility will be large improved comparing with phosphorene

since the carrier mobility is proportional to the elastic modulus. This can be understand as there is suppression of out-of-plane vibration mode due to the flat h-BN, which reduce the stop band in heterostructure. As a consequence, our model will be a good approximation to the experiment in Ref. [7].

In addition, interactions between the carriers and the acoustical vibrations dominate the mobilities of electrons and holes in pure materials. The carriers interact only with those acoustical vibrational modes of long wave-length whose properties are determined by the elastic modulus [51, 52]. The acoustical sound velocity s_l in long wave-length limit is connected to the elastic modulus C via $s_l = C/\rho^{1/2} = (\partial/\partial k)\omega(k)$ with ρ being the mass density and $\omega(k)$ the phonon frequency. By stacking phosphorene on h-BN substrate, the 2D elastic moduli are increased by inheriting the elastic property of h-BN, directly increasing the acoustical sound velocity. The corresponding phonon wave-length of P/h-BN is thus decreased, reducing the effective electron-phonon scattering. As a result, the carrier mobilities of P/h-BN are enhanced. This is not surprising. When a soft material is placed on a hard substrate, the lattice vibration of such stacked heterostructure is determined by the hard substrate and is thus suppressed. This demonstrates the underlying mechanism of the enhanced carrier mobility in P/h-BN, which is in contrast to the theory laying emphasis on the increased damping of Coulombic scattering through modifying the dielectric environments [11]. At the same time, we also found that the 2D elastic modulus of SiO_2 is smaller than those of h-BN. Based on the above discussion, we can infer that the carrier mobilities of phosphorene on h-BN are larger than those on SiO_2.

On the other hand, the h-BN as a substrate, in experiment must be few-layer or even thin film, and so as the phosphorene thin film. To further test the accurate of our model, we construct other two heterostructure to compare with our P/h-BN model, that is monolayer phosphorene on top of bilayer h-BN (P/2h-BN) heterostructure and bilayer phosphorene on monolayer h-BN (2P/h-BN). The carrier mobilities of P/2h-BN and 2P/h-BN heterostructures are shown in Tab. I. The m^* is quite similar to that of P/h-BN heterostructure, and so as the elastic modulus. It can be seen that the C_{2D} of 2P/h-BN and P/2h-BN seem to be effective elastic constant of individual layers, two layers phosphorene and one layer h-BN in 2P/h-BN and one layer phosphorene and two layers h-BN in P/2h-BN. This can be understand classically that two springs of two different spring constant (phosphorene and h-BN) are parallel and the equivalent spring constant is sum of them. Due to the largely

enhanced elastic moduli, the carrier mobilities of 2P/h-BN and P/2h-BN are improved comparing with that of phosphorene. Thus we draw a conclusion that the larger carrier mobility of phosphorene in Ref. [7] comparing with the previous results are derived from the h-BN substrate which induce the elastic modulus to the heterostructure. It is also noticed that the carrier mobilities of 2P/h-BN and P/2h-BN heterostructures are smaller than that of P/h-BN heterostructure, though their elastic moduli are larger. This is because that deformation potential make more important role as the layer increasing. Fortunately, this layer stacking effect of E_i is ignorable in P/h-BN comparing with the increase of the C_{2D}. Hence, in our model, the large enhancement of carrier mobility in phosphorene is from the P/h-BN heterostructure where the h-BN substrate introduces large elastic modulus.

Finally, we should emphasize two points. One is referred to the 2D elastic modulus induced high carrier mobility, which does not increase monotonously with the thickness of substrate. This is because the carrier mobility is also related to the deformation potential. Generally speaking, the deformation potential is the energy change of the VBM and CBM during strains being applied, it increases with the vdW stacking, which will suppress the carrier mobility. Another is referred to the predicted carrier mobilities in our work, which are much larger than those reported experimentally. This is mainly caused by the introduction of impurity or/and vacancy during the synthesis process of phosphorene in experiment. We believe the carrier mobility will be largely improved if phosphorene is prepared with high quality [53].

CONCLUSIONS

In conclusion, we have performed first-principles calculations on the P/h-BN heterostructure to reveal the mechanism of the enhaced carrier mobility in phosphorene on h-BN substrate. The enhanced carrier mobility is demonstrated to be correlated with the increased 2D elastic moduli inherited from the h-BN substrate. The unique electronic properties of phosphorene are almost preserved in the P/h-BN heterostructure, which is due to the weak vdW interactions between phosphorene and h-BN. Our results inevitably offer a new perspective to improve the carrier mobilities in phosphorene field effect transistors.

ACKNOWLEDGMENTS

We would like to thank Zhen Zhu (MSU) for valuable communications. This work was supported by the National Basic Research Program of China under Grant No. 2012CB933101 and the National Science Foundation under Grant No. 51372107, No. 11104122 and No. 51202099. This work was also supported by the National Science Foundation for Fostering Talents in Basic Research of the National Natural Science Foundation of China.

*sims@lzu.edu.cn

[1] X. Ling, H. Wang, S. Huang, F. Xia and M. S Dresselhaus, *PNAS*, 2015, **112**, 4523; See also references therein.

[2] H. Liu, A. T. Neal, Z. Zhu, Z. Luo, X. Xu, D. Tománek and P. D Ye, *ACS Nano*, 2014, **8**, 4033.

[3] B. Radisavljevic, A. Radenovic, J. Brivio, V. Giacometti and A. Kis, *Nat. Nanotech.*, 2011, **6**, 147-150.

[4] J. Qiao, X. Kong, Z.-X. Hu, F. Yang and W. Ji, *Nat. Commun.*, 2014, **5**, 4475.

[5] N. Dasgupta and A. DasGupta, *Semiconductor Devices: Modelling and Technology*, Prentice-Hall of India Pvt. Ltd., Delhi, ISBN 81-203-2398-X, 2004.

[6] Q. H. Wang, K. Kalantar-Zadeh, A. Kis, J. N. Coleman and M. S. Strano, *Nat. Nanotech.*, 2012, **7**, 699-712.

[7] L. Li, G. J. Ye, V. Tran, R. Fei, G. Chen, H. Wang, J. Wang, K. Watanabe, T. Taniguchi, L. Yang, X. H. Chen and Y. Zhang, *Nat. Nanotech.*, 2015, **10**, 608-613.

[8] G. Long, S. G. Xu, Z. F. Wu, T. Y. Han, J. X. Z. Lin, J. Y. Shen, Y. Han, W. K. Wong, J. Q. Hou, R. Lortz and N. Wang, 2016, arXiv:cond-mat.mes-hall/1510.06518.

[9] L. Li, Y. Yu, G. J. Ye, Q. Ge, X. Ou, H. Wu, D. Feng, X. H. Chen and Y. Zhang, *Nat. Nanotech.*, 2014, **9**, 372-377.

[10] F. Xia, H. Wang and Y. Jia, *Nat. Commun.*, 2014, **5**, 4458.

[11] D. Jena and A. Konar, *Phys. Rev. Lett.*, 2007, **98**, 136805.

[12] L. A. Ponomarenko, R. Yang, T. M. Mohiuddin, M. I. Katsnelson, K. S. Novoselov, S. V. Morozov, A. A. Zhukov, F. Schedin, E. W. Hill and A. K. Geim, *Phys. Rev. Lett.*, 2009, **102**,

206603.

[13] A. Konar, T. Fang and D. Jena, *Phys. Rev. B*, 2010, **82**, 115452.

[14] E. Artacho, E. Anglada, O. Diéguez, J. D. Gale, A. García, J. Junquera, R. M. Martin, P. Ordejón, J. M. Pruneda, D. Sánchez-Portal and J. M. Soler, *J. Phys.: Condens. Matter*, 2008, **20**, 064208.

[15] J. P. Perdew, K. Burke and M. Ernzerhof, *Phys. Rev. Lett.*, 1996, **77**, 3865.

[16] J. Klimes, D. R. Bowler and A. Michaelides, *J. Phys.: Condens. Matter*, 2010, **22**, 022201.

[17] D. M. Ceperley and B. J. Alder, *Phys. Rev. Lett.*, 1980, **45**, 566-569.

[18] K. Lee, E. D. Murray, L. Kong, B. I. Lundqvist and D. C. Langreth, *Phys. Rev. B*, 2010, **82**, 081101.

[19] V. R. Cooper, *Phys. Rev. B*, 2010, **81**, 161104.

[20] J. Isberg, J. Hammersberg, E. Johansson, T. Wikström, D. J. Twitchen, A. J. Whitehead, S. E. Coe and G. A. Scarsbrook, *Science*, 2002, **297**, 1670.

[21] E. H. Hwang and S. Sarma, *Phys. Rev. B*, 2008, **77**, 115449.

[22] S. Takagi, A. Toriumi, M. Iwase and H. Tango, *IEEE Trans. Electron Devices*, 1994, **41**, 2363.

[23] S. Bruzzone and G. Fiori, *Appl. Phys. Lett.*, 2011, **99**, 222108.

[24] Z. Zhang, J. Xie, D. Yang, Y. Wang, M. Si and D. Xue, *Appl. Phys. Express*, 2015, **8**, 055201.

[25] Z. Yu, Z. -Y. Ong, Y. Pan, Y. Cui, R. Xin, Y. Shi, B. Wang, Y. Wu, T. Chen, Y. -W. Zhang, G. Zhang and X. Wang, *Advanced Materials*, 2016, **28**, 547-552.

[26] R. Fei, and L. Yang, *Appl. Phys. Lett.*, 2014, **105**, 083120.

[27] Y. Cai, Q. Ke, G. Zhang, Y. P. Feng, V. B. Shenoy and Y.-W. Zhang, *Adv. Funct. Mater*, 2015, **25**, 2230-2236.

[28] J. E. Padilha, A. Fazzio and A. J. R. da Silva, *Phys. Rev. Lett.*, 2015, **114**, 066803.

[29] P. Rivero, C. M. Horvath, Z. Zhu, J. Guan, D. Tománek and S. Barraza-Lopez, *Phys. Rev. B*, 2015, **91**, 115413.

[30] Y. Cai, G. Zhang and Y.-W. Zhang, *J. Phys. Chem. C*, 2015, **119**, 13929.

[31] Y. Cai, G. Zhang and Y.-W. Zhang, *Sci. Rep.*, 2014, **4**, 6677.

[32] J. Dai and X. C. Zeng, *J. Phys. Chem. Lett.*, 2014, **5**, 1289.

[33] C.-R. Hsing, C. Cheng, J.-P. Chou, C.-M. Chang and C.-M. Wei, *N. J. Phys.*, 2014, **16**, 113015.

[34] L. Shulenburger, A. D. Baczewski, Z. Zhu, J. Guan and D. Tománek, *Nano Lett.*, 2015, **15**,

8170.

[35] A. S. Rodin, A. Carvalho and A. H. Castro Neto, *Phys. Rev. Lett.*, 2014, **112**, 176801.

[36] C. Herring, *Phys. Rev.*, 1937, **52**, 365-373.

[37] T. Hu and J. Hong, *ACS Appl. Mater. Interfaces*, 2015, **7**, 23489-23495.

[38] N. W. Ashcroft and N. D. Mermin, *Solid State Physics* Saunders College, Philadelphia, 1976.

[39] F. H. Pollak, M. Cardona, C. W. Higginbotham, F. Herman and J. P. Van Dyke, *Phys. Rev. B*, 1970, **2**, 352.

[40] A. K. Geim and I. V. Grigorieva, *Nature*, 2013, **499**, 419.

[41] F. Bachhuber, J. von Appen, R. Dronskowski, P. Schmidt, T. Nilges, A. Pfitzner and R. Weihrich, *Angew. Chem. Int. Ed.*, 2014, **53**, 11629.

[42] L. Song, L. Ci, H. Lu, P. B. Sorokin, C. Jin, J. Ni, A. G. Kvashnin, D. G. Kvashnin, J. Lou, B. I. Yakobson and P. M. Ajayan, *Nano Lett.*, 2010, **10**, 3209.

[43] C. Lee, X. Wei, W. J. Kysar and J. Hone, *Science*, 2008, **321**, 385.

[44] K. N. Kudin, G. E. Scuseria and B. I. Yakobson, *Phys. Rev. B*, 2001, **64**, 235406.

[45] W. Walukiewicz, H. Ruda, J. Lagowski, and H. Gatos, *Phys. Rev. B*, 1984, **30**, 4571-4582.

[46] Z. Zhu and D. Tománek, *Phys. Rev. Lett.*, 2014, **112**, 176802.

[47] A. Jain and Alan J. H. McGaughey, *Sci. Rep.*, 2015, **5**, 08501.

[48] K. H. Michel and B. Verberck, *Phys. Rev. B*, 2011, **83**, 115328.

[49] S. Jung, M. Park, J. Park, T.-Y. Jeong, H.-J. Kim, K. Watanabe, T. Taniguchi, D. H. Ha, C. Hwang and Y.-S. Kim, *Sci. Rep.*, 2015, **5**, 16642.

[50] A. J. H. McGaughey and M. I. Hussein, *Phys. Rev. B*, 2006, **74**, 104304.

[51] J. Bardeen and W. Shockley, *Phys. Rev.*, 1950, **80**, 72.

[52] W. Shockley and J. Bardeen, *Phys. Rev.*, 1950, **77**, 407.

[53] K. S. Novosolov, V. I. Fal'ko, L. Colombo, P. R. Gellert, M. G. Schwab and K. Kim, *Nature*, 2012, **490**, 192-200.

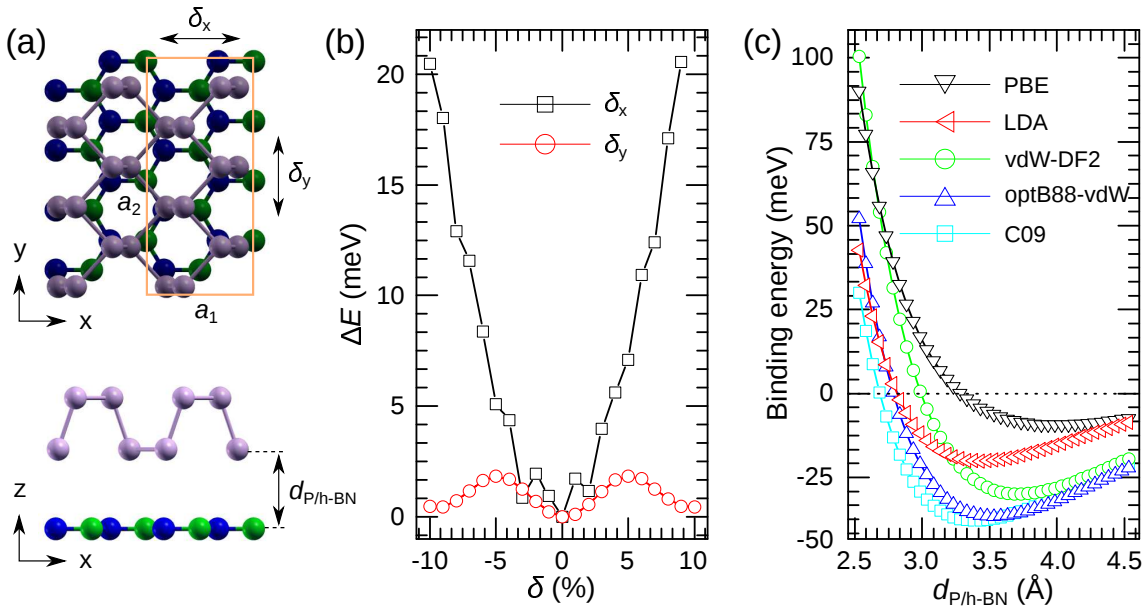

FIG. 1. (color online). (a) Top (top panel) and side (bottom panel) views of P/h-BN heterostructure. The wihte, blue and green balls represent phosphorus, boron and nitrogen atoms, respectively. The yellow rectangle represents the unit cell with $a_1 = 4.54$ Å and $a_2 = 10.04$ Å. δ_x and δ_y are the relative displacements of phosphorene to h-BN. $d_{\mathrm{P/h-BN}}$ is defined as the distance between the phosphorene and h-BN layers. (b) Total energy change as a function of displacements δ_x and δ_y. The functional of optB88-vdW is taken in this calculation. (c) Binding energy per atom as a function of the interlayer spacing $d_{\mathrm{P/h-BN}}$ for five exchange-correlation functionals.

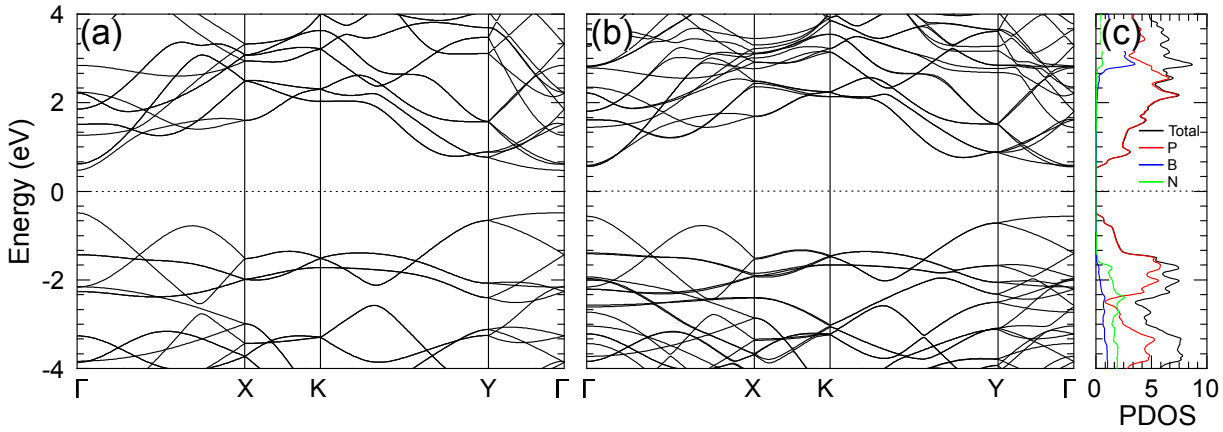

FIG. 2. (color online). Band structures of (a) phosphorene and (b) P/h-BN heterostructure. (c) Projected density of states (PDOS) of P/h-BN, where the black, red, blue, and green lines represent the total density of states, P-, B-, and N-PDOS, respectively. The Fermi level is set to energy zero.

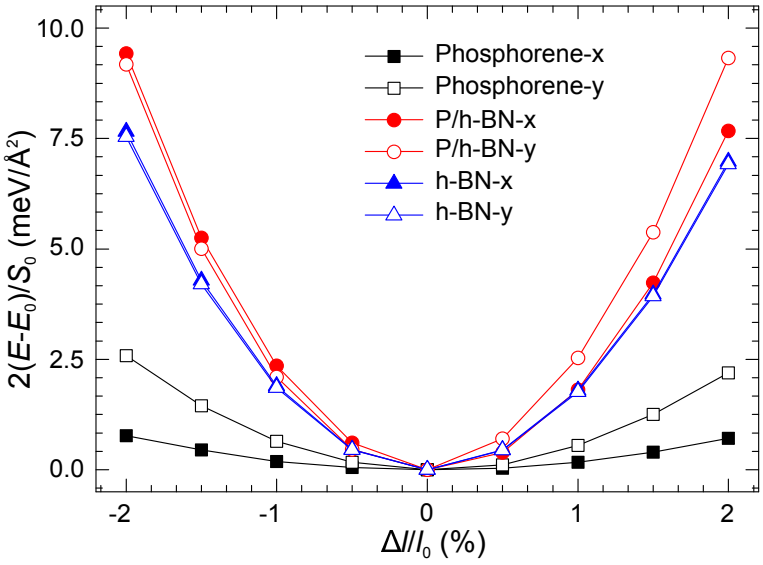

FIG. 3. (color online). The 2D elastic moduli are obtained by fitting the strain energy density curves $2(E - E_0)/S_0$ versus $\Delta l/l_0$ for phosphorene, P/h-BN and h-BN. The strain is applied along the x and y directions.

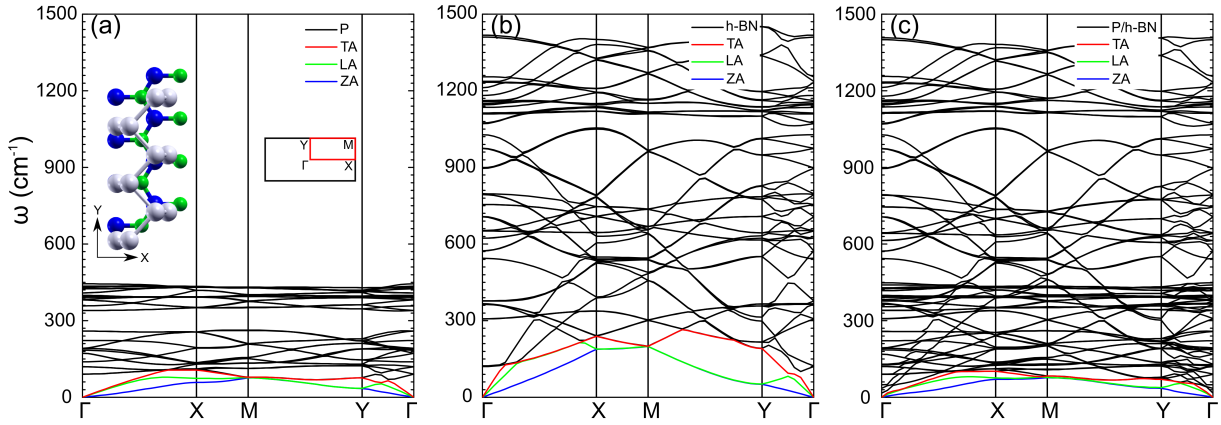

FIG. 4. (color online). The phonon dispersion of phosphorene (a), hexagonal boron nitride (b), and P/h-BN heterostructure (c). The inset figure in (a) is the atomic structure and Brillouin zone of the P/h-BN heterostructure. To be more comparable, the phonon spectrum are in the same scale.

TABLE I. The predicted carrier mobilities of P/h-BN heterostructure , phosphorene and P/2h-BN heterostructure. Types "e" and "h" represent the "electron" and "hole", respectively. $m^*_{x/y}$ (in unit of free electron mass m_0) is the effective mass along the Γ-X/Γ-Y direction. $C_{x/y-2D}$ is the 2D elastic modulus for the Γ-X/Γ-Y direction which is in unit of Jm^{-2}. $E_{ix/y}$ (in unit of eV) is the deformation potential at the Γ point along the Γ-X/Γ-Y direction. $\mu_{x/y-2D}$ (in unit of 10^3 $cm^2V^{-1}s^{-1}$) is the carrier mobility along the Γ-X/Γ-Y direction at room temperature. It is also noticed that the carrier mobilities of phosphorene are calculated in a supercell as same as that used in P/h-BN. And the results are similar to those calculated in a unit cell.

Material	type	m^*_x	m^*_y	C_{x-2D}	C_{y-2D}	E_{ix}	E_{iy}	μ_{x-2D}	μ_{y-2D}
phosphorene	e	0.16	1.31	30.24	96.16	1.49	6.01	4.00	0.09
	h	0.15	3.28	30.24	96.16	2.80	0.58	0.79	2.67
P/h-BN	e	0.21	0.43	321.41	369.86	2.21	6.58	22.34	1.42
	h	0.18	2.99	321.41	369.86	2.83	0.24	6.53	59.96
2P/h-BN	e	0.22	0.31	357.29	466.41	3.68	6.64	8.57	2.44
	h	0.18	1.78	357.29	466.41	2.73	1.37	7.80	4.09
P/2h-BN	e	0.20	0.67	555.52	648.00	2.09	6.71	37.32	1.26
	h	0.18	3.74	555.52	648.00	2.71	0.71	11.00	9.00